RSC Advances

PAPER

View Article Online
View Journal | View Issue

Cite this: *RSC Adv.*, 2024, **14**, 34804

Dual light-responsive shape transformations of a nanocomposite hydrogel sheet enabled by *in situ* etching shaped plasmonic nanoparticles†

Hongyu Guo, *[a] Qiao Ding,[b] Yang Yang,[c] Chenguang Du[d] and Zhihong Nie *[e]

We report here on dual shape transformations of the same thermo-responsive hybrid hydrogel sheet under irradiation of a laser with two different wavelengths (808 nm and 450 nm). By *in situ* etching the silver nanoprisms in the sheet to silver nanodiscs by using chloride ions (Cl^-), two areas with distinct light extinction properties are integrated in a single sheet. The conversion of photon energy to thermal energy in local areas by the silver nanoprisms or nanodiscs under laser irradiation with an appropriate wavelength heats up the sheet locally and causes a local volumetric shrinkage, and hence a volumetric mismatch in different areas in the sheet. The sheet then transforms in a specific way to accommodate this volumetric mismatch. Different patterns of silver nanoprisms and nanodiscs in the sheet are achieved by controlling the delivery patterns of the etchant Cl^-. We demonstrate that by designing the distribution pattern of silver nanoprisms and nanodiscs in the sheet, the same hybrid sheet transforms either to a saddle or to a helical twisted shape, while with another type of distribution pattern, it transforms either to a hoof-like or to a boat-like shape under the irradiation of a laser with a wavelength of either 808 nm or 450 nm. We point out that to program arbitrary curvature of the transformed shape of our sheet, the pattern size of silver nanoprisms and nanodiscs (*i.e.* actuation area) in the sheet needs to be largely reduced, which however limits the heat generated and hence the shape transformations. Factors that affect the sheet's shape transformations are discussed and solutions are suggested to enhance its performance. The hybrid sheet may find applications in soft robotics, for example, as a robotic finger.

Received 23rd April 2024
Accepted 22nd October 2024

DOI: 10.1039/d4ra03024a

rsc.li/rsc-advances

1. Introduction

Machining and molding give us objects with various shapes and functions.[1] While shaped objects can be fabricated by using these external forces, they can also be produced *via* the internal forces within them. Nature provides us with plenty of such examples as tissue growth, opening of pine cones, leaf wrinkling, twisting of a seed pod, snap-buckling of a Venus flytrap and many others.[2] Two basic mechanisms underlie these naturally occurring shape transformations driven by the internal forces within the objects. One is the bilayer-type mechanism where a mismatch of volumetric change exists along the thickness-direction of the object[3] and in the other shaping mechanism, a variation in volumetric change is present in the lateral direction of the object (for example, non-Euclidean plates).[4] The mismatch in the volumetric change generates stress variation and the object transforms in a specific manner to accommodate the competition of the bending and stretching energy in it. A wide range of such shape transforming materials are available such as shape memory polymers, liquid crystal materials, and hydrogels, just to name a few.[1,2,5–7] Many environmental cues have been utilized to generate the mismatch of volumetric change in these materials and trigger their shape transformations. These materials have application potentials in many fields, such as biomedicine, soft robotics, aerospace, functional devices, *etc.*[1]

Compared with environmental cues, such as pH,[8] temperature,[9] enzyme,[10] ions,[11] humidity,[12] DNA,[13] electricity,[14] *etc.*, light can be remotely delivered onto the shape-transforming material on demand in a non-contact mode and has its own merits in realizing materials' shape transformations.[15–24] Parameters, for example, light wavelength, optical power density, light

[a]*Jiangxi Key Laboratory for Mass Spectrometry and Instrumentation, East China University of Technology, Nanchang, 330013, P. R. China. E-mail: guohy89@ecut.edu.cn*

[b]*National R&D Center for Freshwater Fish Processing, College of Life Sciences, Jiangxi Normal University, Nanchang, 330022, P. R. China*

[c]*State Key Laboratory of Supramolecular Structure and Materials, Jilin University, Changchun, 130012, P. R. China*

[d]*School of Medicine, University of North Carolina at Chapel Hill, Chapel Hill, North Carolina, USA*

[e]*State Key Laboratory of Molecular Engineering of Polymers, Department of Macromolecular Science, Fudan University, Shanghai, 200438, P. R. China. E-mail: znie@fudan.edu.cn*

† Electronic supplementary information (ESI) available. See DOI: https://doi.org/10.1039/d4ra03024a

irradiation time, polarization, shape of light spot, *etc.*, can be tuned to achieve desired transformation modes from the materials. For example, by controlling the light delivery manner, a single sheet transforms in various ways to achieve desired shapes.[25–27] By integrating organic dyes of different colors with the polymer sheet, the sheet undergoes distinct shape transformations under light irradiation of different wavelengths.[20,28,29] These reconfigurable shape transformations brought by the same sheet increase its adaptive functions.[30] However, it remains an uneasy task to integrate in various ways organic dyes of sharply different colors into the same shape transforming hydrogel material, which have their own advantages in certain settings (such as in biomedicine).[7,9,31–34]

Herein, we report on the shape transformation of a nanocomposite hydrogel sheet under light irradiation of two different wavelengths. Silver nanoprisms are firstly embedded into the thermo-responsive hydrogel sheet during its fabrication. By controlling the delivery pattern of chloride ions (Cl^-) to the sheet, the silver nanoprisms at certain regions are etched by Cl^- to silver nanodiscs (Scheme 1a),[35] making the regions have distinct light extinction properties compared with other areas of the sheet. The photo-thermal effect of either silver nanoprisms or the *in situ* generated silver nanodiscs increase the temperature locally in the sheet under a corresponding laser irradiation, thus bringing in a mismatch of volumetric change, and hence the sheet's shape transformation. Two distinct shape transformations are accomplished from a single sheet under laser irradiation of two different wavelengths (one is 450 nm, the other is 808 nm) for a specific pattern of silver nanoprisms and nanodiscs (Scheme 1b). This pattern can be varied by changing the delivery pattern of Cl^-. The parameters affecting the shape transformations are discussed. The hybrid hydrogel sheet reported herein may find applications in soft robots, for example, as a robotic finger.

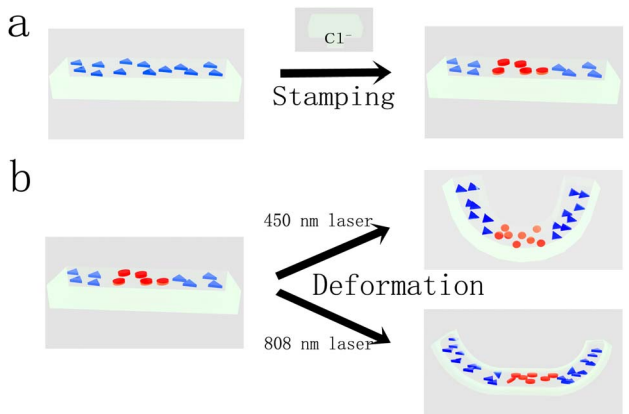

Scheme 1 (a) An agarose hydrogel with chloride ions (Cl^-) is brought in contact to the hybrid hydrogel sheet with embedded silver nanoprisms. After the contact, Cl^- ions diffuse to the sheet and transform *in situ* the silver nanoprisms to silver nanodiscs located in the contact region; (b) the hybrid sheet with patterned silver nanoprism and silver nanodiscs bends in different areas under the laser irradiation with different wavelengths (one is 450 nm, the other is 808 nm).

2. Experimental

2.1. Materials

Silver nitrate ($AgNO_3$), sodium borohydride (analytical grade, $NaBH_4$) and 30% hydrogen peroxide (guaranteed reagent, H_2O_2) were purchased from Sinopharm Chemical Reagent Co., Ltd, China; *N*-isopropyl acrylamide (NIPAM, Adamas-beta), *N*,*N*′-methylenebis (acrylamide) (BIS, Adamas-beta), ammonium persulfate (analytical grade, ≥98.0%, APS, general-reagent) and sodium citrate tribasic dihydrate (analytical grade, ≥99.0%, general-reagent) were supplied by Shanghai Titan Scientific Co., Ltd, China; *N*,*N*,*N*′,*N*′-tetramethylethylenediamine (T105497-25 mL, TEMED) was bought from Shanghai Aladdin Biochemical Technology Co., Ltd, China; potassium chloride (99.5%, KCl) and agarose were purchased from Meryer (Shanghai) Biochemical Technology Co., Ltd, China. All chemicals were used as received. Distilled water was used throughout the experiments.

2.2. Fabrication of silver nanoprisms

The silver nanoprisms were synthesized according to the published paper with an enlarged solution volume.[36] In a 500 mL round-bottom flask were added 200 μL 0.1 M $AgNO_3$, 4 mL 75 mM sodium citrate, 193.84 mL water and 960 μL H_2O_2. The solution was magnetically stirred at 500 rpm. 1 mL of an ice-cold 0.1 M $NaBH_4$ aqueous solution is then added to the flask to initiate the reaction. After stirring the solution for 5 minutes, the solution was left still for at least 2 hours to completely consume the excess of $NaBH_4$ in the solution. The solution was then ready for further use.

2.3. Fabrication of agarose hydrogel

1 g agarose powder was added to 50 mL water in a round-bottom flask. The flask was then heated up to about 95 °C under magnetic stirring to fully dissolve the agarose powder. The hot agarose solution was then poured in a plastic Petri dish and was left to cool down to the room temperature to gelate the agarose solution. The agarose hydrogel was then cut with desired sizes for further use.

2.4. Fabrication of hybrid hydrogel sheet with silver nanoprisms or silver nanodiscs

Eight centrifuge tubes with each containing 12 mL silver nanoprism solution were centrifuged at 10 000 rpm for 15 minutes. The supernatants were removed and the precipitates were combined together in 500 μL water, to which 0.113 g NIPAM monomer and 0.006 g BIS cross-linker were added. Then the solution was purged with nitrogen gas for 5 minutes to remove dissolved oxygen in water. After that, 3 μL 10 wt% APS initiator and 1 μL TEMED catalyst were added to the solution. Then the solution was injected to a pre-cooled glass mold made by two pieces of glass slides and the parafilm spacer. The reaction was left to start in the refrigerator of 4 °C for 30 minutes. The hybrid hydrogel sheet was then removed from the glass mold and immersed in a copious amount of water to leak

out unreacted chemicals. The hybrid sheet with silver nanodiscs was prepared by immersing the sheet with silver nanoprisms in a 0.5 M KCl aqueous solution. For the sheet with patterns of silver nanoprisms and nanodiscs, a piece of agarose hydrogel with desired size was soaked in 0.5 M KCl aqueous solution for at least 1 hour and then contacted the sheet with silver nanoprisms for 1 second. After removing the agarose, the Cl^- ion continues to diffuse in both lateral and thickness-direction of the sheet to locally transform the silver nanoprisms to silver nanodiscs. The hybrid sheet was then used for laser irradiation.

2.5. Laser set-up for shape transformations of the hybrid sheet

A continuous-wave laser was used with either 450 nm wavelength (CME-L450-5W, Microenerg (Beijing) Technology Co., Ltd, China) or 808 nm wavelength (MDL-XF-808nm-10W-DE51801, Changchun New Industries Optoelectronics Tech. Co., Ltd, China). Without special notice, the laser power density was set as 1.7 W cm^{-2} for the laser of an 808 nm wavelength and 4.3 W cm^{-2} for the laser of a 450 nm wavelength. The laser spot covers either the whole hybrid sheet or a portion of the sheet to achieve a desired shape transformation.

2.6. Measurement on swelling property of the hybrid sheet

Three pieces of circular disks were cut out from the hybrid sheet with either silver nanoprisms or silver nanodiscs. The disks were transferred to glass bottles with water, which were then placed in a heat bath. The temperature of the heat bath was adjusted and the hydrogel disks were left in the bath to reach swelling equilibrium. Then their diameters were measured and plotted against the corresponding temperature.

2.7. Light extinction measurement of the hybrid sheet

The light extinction property of the hybrid hydrogel sheet was measured by a UV-vis spectroscopy (SP-752, Shanghai Spectrum Instruments Co., Ltd, China). A piece of hybrid hydrogel sheet with either silver nanoprisms or nanodiscs was cut from the as-made sheets and was immersed in water in the quartz cuvette, vertically contacting one side of the cuvette wall. Then its light extinction at desired wavelengths was measured.

2.8. Scanning electron microscopy of silver nanoprisms and silver nanodiscs

The as-synthesized silver nanoprisms were centrifuged at 10 000 rpm for 15 minutes and re-dispersed in water. Then a drop of the solution was cast on a silicon wafer and left to dry in air. To prepare silver nanodiscs for imaging, 200 μL 0.5 M KCl aqueous solution was added to 24 mL as-made silver nanoprisms solution under stirring. After the reaction finished, the silver nanodiscs solution was centrifuged at 10 000 rpm for 15 minutes and re-dispersed in water. Then a drop of the solution was cast on a silicon wafer and dried in air. The scanning electron microscopy was done by using Nova NanoSEM 450 (FEI, USA).

2.9. Measurement on temperature and bending evolutions of the hybrid sheet under laser irradiation

A T-type thermo-couple (bought from a local supplier from China) with a thickness of 20 μm and a diameter of 0.5 mm was used (Fig. S1b and f†). It was inserted in the hybrid sheet at desired locations (Fig. S1a and c–e†). Then that area of the sheet was irradiated by using laser with different wavelengths. The temperature evolution with time was recorded by the digital thermo meter connected with the thermo-couple, while in the meantime the bending evolution of the sheet was recorded by a camera in video mode. The bending angle of the sheet at different time of laser irradiation was analyzed by ImageJ program and was related with the measured temperature at the same irradiation time.

2.10. Measurement on the laser intensity distribution of the laser spot

Generally, the laser spot has an intensity distribution of a Gaussian type. Here the intensity of the laser spot was roughly analyzed by the thermo-couple. The thermo-couple was immersed in water and placed in different locations of the laser spot along the direction of its diameter (Fig. S2†). Then the thermo-couple was irradiated by the laser of an 808 nm wavelength for 5 seconds. The temperature was recorded and plotted with respect to the location of the thermo-couple within the laser spot.

3. Results and discussions

3.1. Material properties of the hybrid hydrogel sheet

The hybrid hydrogel sheet with either silver nanoprisms or silver nanodiscs shows an extinction of light within certain wavelengths (Fig. 1a). The two light extinction spectra are well separated from each other, with one of the extinction peak centering at 700 nm and the other centering at 440 nm. The scanning electron microscopy measurement verifies the successful synthesis of silver nanoprisms and silver nanodiscs (Fig. 1c and d). The difference in the light extinctions of the sheets with different shaped plasmonic nanoparticles sets a basis for the success in the realization of dual light-responsive shape deformations of the hybrid sheet. With an increase of the temperature, the hybrid sheet with either silver nanoprisms or silver nanodiscs gradually loses water and decreases its volume and mass. This reflects the thermo-responsiveness of PNIPAM hydrogel (Fig. 1b).

3.2. Study on bending deformation of the hybrid hydrogel sheet

The temperature and bending evolutions during laser irradiation were studied for the hybrid sheets with either silver nanoprisms or silver nanodiscs (see Supporting Videos 1 and 2†). A thermo-couple was inserted in the sheet in both cases to study the temperature evolution as the bending occurred. It is found that the temperature in the sheet increases quickly to a maximum (~30 s), well above the LCST of the hybrid PNIPAM hydrogel for both cases, which is ascribed to the photo-thermal

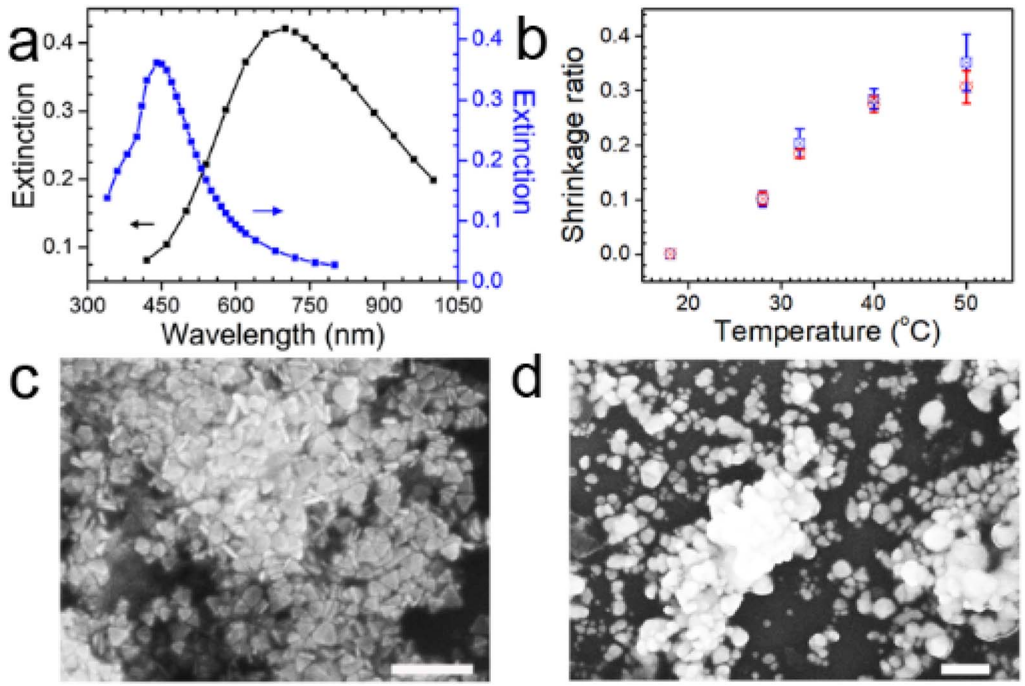

Fig. 1 (a) Light extinction spectrum of the hybrid hydrogel sheet with either silver nanoprisms (black curve) or silver nanodiscs (blue curve); (b) shrinkage property of the hybrid hydrogel sheet with silver nanoprisms (blue symbol) or nanodiscs (red symbol) as a function of temperature; (c) and (d) scanning electron microscopy images of as-synthesized silver nanoprisms and silver nanodiscs that were generated from silver nanoprisms *via* Cl etching, respectively. Scale bar: 200 nm.

conversion of either silver nanoprisms or silver nanodiscs. During this time, the sheets slightly bend (see the second inserted images in Fig. 2a and b). As the laser irradiation continues, the temperature drops a bit but is still above the LCST of the sheet. This indicates a heat dissipation to the surroundings around the thermo-couple. In the end, a stable temperature reaches due to the balance of the heat generation and dissipation. During this evolution of temperature, the sheets gradually bend with a larger degree (see the third inserted images in Fig. 2a and b).

This phenomenon suggests that during laser irradiation, the heat transfer of the sheets occur faster than the mass transfer (*i.e.*, water loss due to temperature-driven volumetric collapse of the hybrid hydrogels). When the laser is shut off (at ~380 s in Fig. 2a and ~132 s in Fig. 2b), the temperature in the sheets quickly decreases (in ~1 min) to a value close to the one before laser irradiation, while an appreciable bending deformation

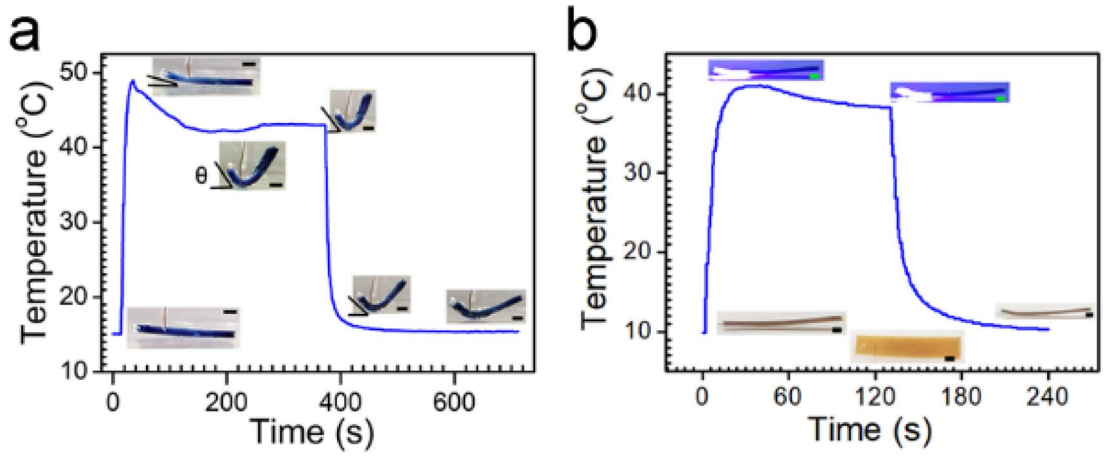

Fig. 2 (a) and (b) Temperature and bending evolutions of the hybrid hydrogel sheet with time during laser irradiation with a wavelength of 808 nm and 450 nm separately. The inserted photo images show the bending state of the sheet at different irradiation time. Scale bar: 3 mm in (a) and 2 mm in (b).

still remains, again suggesting a faster heat transfer than mass transfer. It takes about 40 minutes for the sheets with maximum bending to revert back to the flat states. The bending deformation is reversible and can be repeated for at least 10 times.

The bending deformation of the hybrid hydrogel sheets increases as a function of the laser power density. For example, the bending angle of the sheet with silver nanoprisms increases from 22° to 86° when the laser power density changes from 1.02 to 1.69 W cm^{-2} (Fig. 3a). For the sheet with silver nanodiscs, the bending angle increases from 14° to 96° when the laser power density increases from 1.5 to 4.3 W cm^{-2} (Fig. 3b). When reducing the width of the strip pattern, the bending angle decreases for the hybrid sheet with either silver nanoprisms or silver nanodiscs. For example, the bending angle decreases from 63° to 48° under a laser irradiation of 1.69 W cm^{-2} for the hybrid sheet with silver nanoprisms when the width of the strip pattern drops from 3 mm to 2 mm (Fig. 3c). While for the hybrid sheet with silver nanodiscs, it decreases from 79° to 53° at a laser powder density of 4.3 W cm^{-2} when the width of the strip pattern reduces from 3 mm to 2 mm (Fig. 3d).

3.3. Dual light-responsive shape transformations of the hybrid sheet

The patterning approach used here enables the integration of silver nanoparticles with two different shapes in a single piece of the hydrogel sheet in various forms, resulting in distinct overall transformed shapes under the irradiation of laser with different wavelengths. For example, a rectangular sheet where the silver nanoprisms are located in the middle regions and silver nanodiscs in the side regions transforms to a shape similar to a horse's hoof under the laser irradiation of an 808 nm wavelength (Fig. 4, top right image). The same sheet

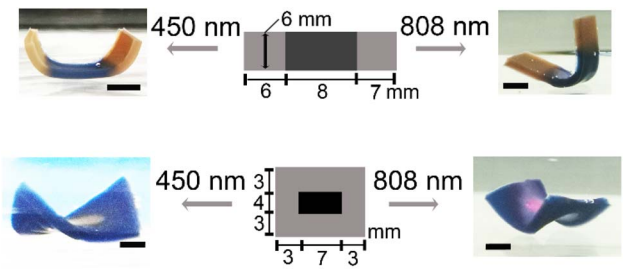

Fig. 4 Dual shape transformations of the hybrid sheet patterned with silver nanoprisms and nanodiscs under laser irradiation at different wavelengths (one is 450 nm and the other is 808 nm). The middle illustrations give the dimensions of the hybrid sheet where the black area denotes the region of silver nanoprisms and the grey area represents the area of silver nanodiscs in the top illustration. In the bottom illustration, the black area denotes the region of silver nanodiscs and the grey area represents the region of silver nanoprism. Scale bar: 6 mm in the top images and 3 mm in the bottom images.

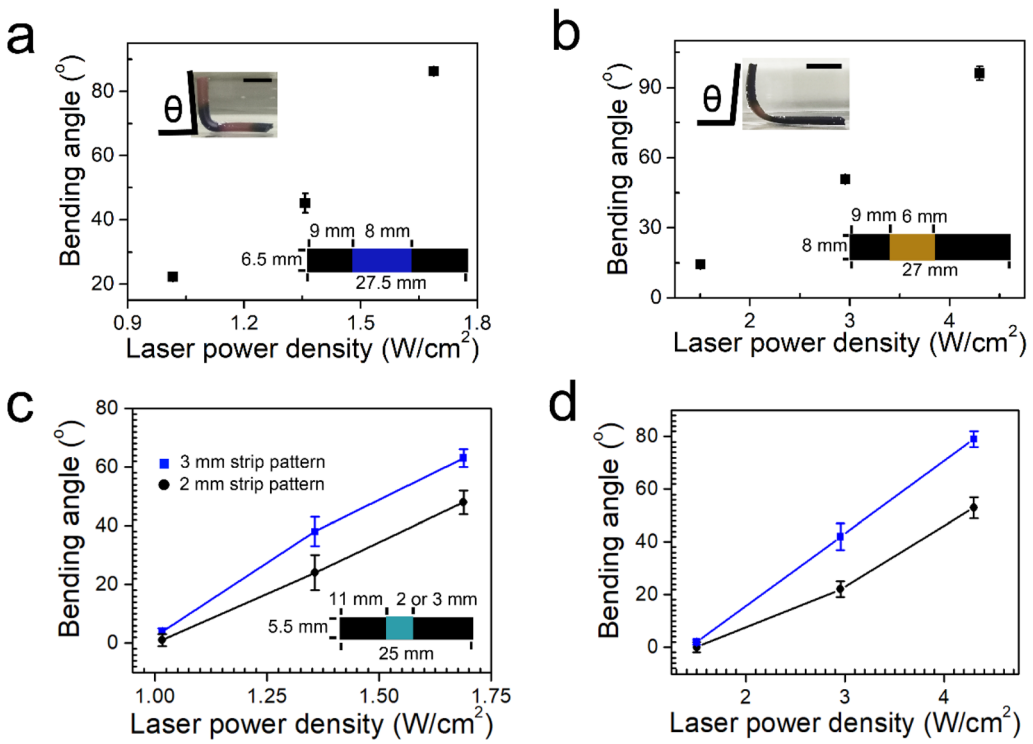

Fig. 3 (a) and (b) Bending angle of the hybrid sheet with silver nanoprisms and nanodiscs as a function of laser power density at a certain wavelength (808 nm in a and 450 nm in (b)), respectively. The inserted photo images in (a) and (b) show the bent sheet and how the bending angle (θ) was measured. The inserted illustrations give the dimensions of the sheet and the actuation area (blue region in a and yellow region in (b)); (c) and (d) bending angle of the hybrid sheet with silver nanoprisms and nanodiscs with different widths of the patterned actuation strip as a function of laser power density at a specific wavelength (808 nm in c and 450 nm in (d)), respectively. The inserted illustrations in (c) give the dimensions of the sheet and the actuation strip (cyan region) used in (c) and (d). Scale bar: 5 mm in (a) and 6 mm in (b).

transforms to a boat-like shape by using a laser irradiation of a 450 nm wavelength (Fig. 4, top left image). For the rectangular sheet where the silver nanodiscs reside in the central areas and are surrounded by silver nanoprisms in the edge areas, it transforms to a helical twisted shape with the laser irradiation of a 450 nm wavelength (Fig. 4, bottom left image), while it shifts to a saddle-like shape in response to a laser irradiation of an 808 nm wavelength (Fig. 4, bottom right image). Other patterns of silver nanoprisms and silver nanodiscs in the sheet can be designed, expanding the transformed shapes accessed by the sheet when lasers with two different wavelengths are used to irradiate it.

3.4. Discussions

The shape transformation of the hybrid sheet with a relatively large thickness (1 mm) is believed to occur *via* a bilayer-type mechanism.[20,26,37–39] During the laser irradiation, the silver nanoprisms or silver nanodiscs in the sheet absorb the laser light, resulting in the decrease of light intensity as the laser passes through the sheet in the thickness direction. As the reduction of laser intensity occurs, the silver nanoprisms or nanodiscs convert the absorbed photons to thermal energy, which accumulates and increases the temperature in the sheet to a value above its LCST after the laser passes through a certain portion of the sheet in the thickness direction. The accumulated heat also dissipates to other areas of the sheet with lower temperature, causing a thermal broadening and a thermal gradient as well in the thickness direction. We note that the actual measurement of the thermal distribution in the sheet's thickness direction remains for the time being a challenging task for us for a sheet with a thickness of 1 mm. The thermal gradient in the thickness direction of the sheet results in a gradient of shrinkage ratio along that direction, leading to a bending deformation in the end to reduce the stretching cost in the sheet. By controlling the distribution of the actuation area in the sheet, more complex shape transformations can be accomplished *via* the competition of the bending and stretching energy in the sheet to minimize its elastic energy. For example, the incoherent bending deformation due to the size difference of the actuation areas around the edges of the sheet leads to a saddle-like shape transformation to resolve their bending competition during the 808 nm laser irradiation (Fig. 4, bottom right image). While the different adaptations of the non-actuation areas to the bending deformation of the actuation area eventually causes a helical twisted shape transformation under 450 nm laser irradiation (Fig. 4, bottom left image).

We mention here that a minimal size of the actuation domain needs to be satisfied for a bending deformation to occur under the laser irradiation at a certain power density for both laser wavelengths (Fig. 3c and d). This is consistent with the previous findings of our and others' work.[20,26,38,39] Generally speaking, the sheet's deformation under laser irradiation for our case relies on the thermal energy converted from the photons absorbed by the silver nanoprisms or nanodiscs. The number of the absorbed photons depends on the molar absorption coefficient at the laser wavelength, thickness of the sheet (*i.e.*, optical path length) and concentration of the nanoparticles according to Lambert–Beer law. In addition to these factors, increasing the size of the actuation domain increases the area that contributes to the accumulation of heat, and hence to the increase of the temperature. This results in an enhanced bending deformation (Fig. 3c and d).[20,26,38]

4. Conclusions

In conclusion, we report here on dual shape transformations of the same thermo-responsive hybrid poly (*N*-isopropyl acrylamide) hydrogel sheet under irradiation of laser with two different wavelengths (one is 808 nm and the other is 450 nm). By *in situ* etching the silver nanoprisms in the sheet to silver nanodiscs by using chloride ion (Cl^-), two areas with distinct light extinction properties are integrated in a single sheet, setting a foundation for the realization of its dual shape transformations by using lasers. The conversion of photon energy to thermal energy in local areas by the silver nanoprisms or nanodiscs under laser irradiation with a proper wavelength heats up the sheet locally and causes a local volumetric shrinkage, and hence a volumetric mismatch in different areas in the sheet. The sheet then transforms in a specific way to accommodate this volumetric mismatch. Different distributions of silver nanoprisms and nanodiscs in the sheet are achieved by controlling the delivery patterns of the etchant Cl^-. We demonstrate that by designing the distribution pattern of silver nanoprisms and nanodiscs in the sheet, the same hybrid sheet transforms either to a saddle or to a helical twisted shape, while with another type of distribution pattern, it transforms either to a hoof-like or to a boat-like shape under the irradiation of laser with different wavelengths (one is 808 nm and the other is 450 nm).

We point out that to program arbitrary curvature of the transformed shape of our sheet,[40,41] the pattern size of silver nanoprisms and nanodiscs (*i.e.*, actuation area) in the sheet needs to be largely reduced. However, reducing the domain size of silver nanoprisms and nanodiscs in the sheet limits the heat generated in that domain and hence the temperature rise there under laser irradiation, which in some cases does not enable a deformation to occur.[20,26,38,39] Several factors can be considered to overcome this problem:[23] (1) matching the laser wavelength with the peak absorption wavelength of the photo-thermal nanoparticles; (2) enhancing the photo-thermal conversion capability of the nanoparticles and reducing their light scattering; (3) increasing the loading of the nanoparticles in the sheet.

We also point out that the laser intensity distribution in the laser spot needs to be considered as well to achieve curvatures from the planar sheet in a more predictable manner. This is because the transformation of sheet can either bring the initially non-irradiated area to laser exposure[25,26,38] or increase the laser intensity on the irradiated area due to the Gaussian-type intensity distribution of the laser spot (Fig. S2†). Also instead of changing the laser irradiation area of the patterned sheet from time to time to achieve a desired shape, it is more

favorable to shed a laser irradiation on the whole actuation areas to realize shape transformations in a more reproducible manner. The hybrid sheet reported herein may find applications in soft robotics, for example, as a robotic finger.

Data availability

The data are available from the corresponding author on reasonable request.

Conflicts of interest

There are no conflicts to declare.

Acknowledgements

We acknowledge the support from the start-up fund from East China University of Technology (no. DHBK2019259).

References

1 Y. Liu, J. Genzer and M. D. Dickey, *Prog. Polym. Sci.*, 2016, **52**, 79–106.
2 L. M. de Espinosa, W. Meesorn, D. Moatsou and C. Weder, *Chem. Rev.*, 2017, **117**, 12851–12892.
3 R. M. Erb, J. S. Sander, R. Grisch and A. R. Studart, *Nat. Commun.*, 2013, **4**, 1712.
4 E. Sharon and E. Efrati, *Soft Matter*, 2010, **6**, 5693–5704.
5 T. J. White and D. J. Broer, *Nat. Mater.*, 2015, **14**, 1087–1098.
6 Q. Zhao, H. J. Qi and T. Xie, *Prog. Polym. Sci.*, 2015, **49–50**, 79–120.
7 S.-J. Jeon, A. W. Hauser and R. C. Hayward, *Acc. Chem. Res.*, 2017, **50**, 161–169.
8 Q. Zhao, X. X. Yang, C. X. Ma, D. Chen, H. Bai, T. F. Li, W. Yang and T. Xie, *Mater. Horiz.*, 2016, **3**, 422–428.
9 G. Stoychev, C. Reuther, S. Diez and L. Ionov, *Angew. Chem., Int. Ed.*, 2016, **55**, 16106–16109.
10 J. C. Athas, C. P. Nguyen, B. C. Zarkett, A. Gargava, Z. H. Nie and S. R. Raghavan, *ACS Appl. Mater. Interfaces*, 2016, **8**, 19066–19074.
11 E. Palleau, D. Morales, M. D. Dickey and O. D. Velev, *Nat. Commun.*, 2013, **4**, 2257.
12 H. Arazoe, D. Miyajima, K. Akaike, F. Araoka, E. Sato, T. Hikima, M. Kawamoto and T. Aida, *Nat. Mater.*, 2016, **15**, 1084–1089.
13 A. Cangialosi, C. Yoon, J. Liu, Q. Huang, J. K. Guo, T. D. Nguyen, D. H. Gracias and R. Schulman, *Science*, 2017, **357**, 1126–1129.
14 C. J. Yu, Z. Duan, P. X. Yuan, Y. H. Li, Y. W. Su, X. Zhang, Y. P. Pan, L. L. Dai, R. G. Nuzzo, Y. G. Huang, H. Q. Jiang and J. A. Rogers, *Adv. Mater.*, 2013, **25**, 1541–1546.
15 M. R. Shankar, M. L. Smith, V. P. Tondiglia, K. M. Lee, M. E. McConney, D. H. P. Wang, L. S. Tan and T. J. White, *Proc. Natl. Acad. Sci. U. S. A.*, 2013, **110**, 18792–18797.
16 A. H. Gelebart, D. J. Mulder, M. Varga, A. Konya, G. Vantomme, E. W. Meijer, R. L. B. Selinger and D. J. Broer, *Nature*, 2017, **546**, 632–636.
17 J. A. Lv, Y. Y. Liu, J. Wei, E. Q. Chen, L. Qin and Y. L. Yu, *Nature*, 2016, **537**, 179–184.
18 S. Palagi, A. G. Mark, S. Y. Reigh, K. Melde, T. Qiu, H. Zeng, C. Parmeggiani, D. Martella, A. Sanchez-Castillo, N. Kapernaum, F. Giesselmann, D. S. Wiersma, E. Lauga and P. Fischer, *Nat. Mater.*, 2016, **15**, 647–653.
19 L. D. Zhang, H. R. Liang, J. Jacob and P. Naumov, *Nat. Commun.*, 2015, **6**, 7429.
20 Y. Liu, B. Shaw, M. D. Dickey and J. Genzer, *Sci. Adv.*, 2017, **3**, e1602417.
21 D. D. Han, Y. L. Zhang, J. N. Ma, Y. Q. Liu, B. Han and H. B. Sun, *Adv. Mater.*, 2016, **28**, 8328–8343.
22 Y. Zhou, A. W. Hauser, N. P. Bende, M. G. Kuzyk and R. C. Hayward, *Adv. Funct. Mater.*, 2016, **26**, 5447–5452.
23 T. Wang, D. Torres, F. E. Fernández, C. Wang and N. Sepúlveda, *Sci. Adv.*, 2017, **3**, e1602697.
24 T. Ikegami, Y. Kageyama, K. Obara and S. Takeda, *Angew. Chem., Int. Ed.*, 2016, **55**, 8239–8243.
25 A. W. Hauser, A. A. Evans, J. H. Na and R. C. Hayward, *Angew. Chem., Int. Ed.*, 2015, **54**, 5434–5437.
26 H. Y. Guo, J. Cheng, J. Y. Wang, P. Huang, Y. J. Liu, Z. Jia, X. Y. Chen, K. Y. Sui, T. Li and Z. H. Nie, *J. Mater. Chem. B*, 2017, **5**, 2883–2887.
27 A. S. Kuenstler, M. Lahikainen, H. T. Zhou, W. W. Xu, A. Priimagi and R. C. Hayward, *ACS Macro Lett.*, 2020, **9**, 1172–1177.
28 A. H. Gelebart, D. J. Mulder, G. Vantomme, A. Schenning and D. J. Broer, *Angew. Chem., Int. Ed.*, 2017, **56**, 13436–13439.
29 B. Zuo, M. Wang, B. P. Lin and H. Yang, *Nat. Commun.*, 2019, **10**, 4539.
30 O. Kuksenok and A. C. Balazs, *Adv. Funct. Mater.*, 2013, **23**, 4601–4610.
31 L. Ionov, *Mater. Today*, 2014, **17**, 494–503.
32 C. Lowenberg, M. Balk, C. Wischke, M. Behl and A. Lendlein, *Acc. Chem. Res.*, 2017, **50**, 723–732.
33 K. Baek, J. H. Jeong, A. Shkumatov, R. Bashir and H. Kong, *Adv. Mater.*, 2013, **25**, 5568–5573.
34 M. Jamal, S. S. Kadam, R. Xiao, F. Jivan, T. M. Onn, R. Fernandes, T. D. Nguyen and D. H. Gracias, *Adv. Healthc. Mater.*, 2013, **2**, 1142–1150.
35 J. An, B. Tang, X. Zheng, J. Zhou, F. Dong, S. Xu, Y. Wang, B. Zhao and W. Wu, *J. Phys. Chem. C*, 2008, **112**, 15176–15182.
36 Q. Zhang, N. Li, J. Goebl, Z. Lu and Y. Yin, *J. Am. Chem. Soc.*, 2011, **133**, 18931–18939.
37 Y. Yang, Z. Q. Pei, Z. Li, Y. Wei and Y. Ji, *J. Am. Chem. Soc.*, 2016, **138**, 2118–2121.
38 H. Y. Guo, Y. J. Liu, Y. Yang, G. Y. Wu, K. Demella, S. R. Raghavan and Z. H. Nie, *J. Mater. Chem. B*, 2019, **7**, 1679–1683.
39 H. Y. Guo, J. Cheng, K. K. Yang, K. Demella, T. Li, S. R. Raghavan and Z. H. Nie, *ACS Appl. Mater. Interfaces*, 2019, **11**, 42654–42660.
40 J. Kim, J. A. Hanna, M. Byun, C. D. Santangelo and R. C. Hayward, *Science*, 2012, **335**, 1201–1205.
41 T. H. Ware, M. E. McConney, J. J. Wie, V. P. Tondiglia and T. J. White, *Science*, 2015, **347**, 982–984.